

Properties of individual Asian dust storm particles collected at Kosan, Korea during ACE-Asia

Chang-Jin Ma^{a,*}, Susumu Tohno^a, Mikio Kasahara^a, Shinjiro Hayakawa^b

^aDepartment of Socio-Environmental Energy Science, Graduate School of Energy Science, Kyoto University, Uji, Kyoto 611-0011, Japan

^bGraduate School of Engineering, Hiroshima University, Higashi-Hiroshima, Hiroshima 739-8527, Japan

Received 17 June 2003; accepted 24 November 2003

Abstract

For the purpose of studying the properties of individual Asian dust storm particles, an intensive field measurement took place at the Kosan ground-based station located on the west coast of Cheju Island, Korea during ACE-Asia campaign. A 2-stage filter pack sampler was employed in the size-resolved (coarse and fine fractions) particle sampling. The trace elements of individual coarse particles ($> 1.2 \mu\text{m}$) were analyzed by the X-ray microprobe analysis system equipped at SPRING-8. The result of statistical analysis suggested that individual particles collected in Asian dust storm event could be classified into four groups: sea-salt-rich particles, crustal-rich particles, crustal/sea-salt/sulfur-rich particles, and crustal/sea-salt-rich particles. Moreover, according to the XRF elemental maps and elemental masks replayed corresponding to individual particles, particles could be categorized into two groups, namely internally mixed particles and externally mixed particles. A small part of the CaCO_3 in Asian dust storm particles would be converted to CaSO_4 through the chemical reaction between CaCO_3 and H_2SO_4 during long-range transport. By means of XANES method, the major chemical state of Fe in Fe-rich particles was found to be Fe^{3+} . Several minor trace heavy metals were probably affected by the air masses passed directly over the industrial areas of China.

© 2003 Elsevier Ltd. All rights reserved.

Keywords: Asian dust storm; Individual particles; X-ray microprobe system; Elemental mass; ACE-Asia

1. Introduction

As one of the international global atmospheric research programs for understanding the composition, source, transport, deposition, and transformation of Asian dust storm and its impacts on the environment, Aerosol Characterization Experiment (ACE)-Asia was intensively performed during the spring of 2001. The detailed measurements such as chemistry, physics, and optical properties for Asian dust storm particles at ground-based, ship, aircraft, and satellite improved our understanding of the properties and impacts of Asian dust storm particles.

In the spring, conditions in the atmosphere over Asia are ripe for both massive dust storms and wholesale movement of large volumes of air across the Pacific Ocean. The combination of dry soils and high winds leads to a spurt of dust storm activity, which coincides with strong winds that carry the dust over the Pacific. This Asian dust storm is a serious and growing environmental problem in East Asia as well as the Pacific Basin.

Chemical analysis of airborne particles is usually carried out by collecting a sample of many particles on a filter or impactor stage, and using bulk analytical methods to deduce composition. These methods obscure the particle-to-particle composition variations. Since a long sampling duration time is required for particle analysis using the commercially available aerosol instrumentation, the particle composition may be

*Corresponding author. Tel.: +81-774-38-4413; fax: +81-774-38-4411.

E-mail address: ma@uji.energy.kyoto-u.ac.jp (C.-J. Ma).

altered during the collection process due to condensation or evaporation of volatile compounds, or chemical reactions. From this point of view, one of the advantages of single-particle analysis technique is that it is not necessary to carry out sampling for a long time. It is important to understand the distribution and transport of trace elements by airborne particulates including primary sources of various elements.

Several types of mathematical models have been used in the source apportionment of environmental samples. For quantitative analyses, chemical mass balance (CMB) and multivariate models were developed. As one of multivariate statistical techniques, factor analysis has been commonly used in environmental studies to identify sources from the data taken at receptors (Lowenthal and Rahn, 1987; Christof et al., 1992; Olmez et al., 1994; Huang et al., 1999). From the matrixes of correlation or covariance, factor analysis generates a few underlying “factors” that describe groups of variables (Huang et al., 1999). However, as one of the disadvantages of multivariate model, it does require a large range of analyses. Moreover, to obtain a satisfactory analysis result, one has to take into account gas-to-particle transformations and coagulation and growth processes as well as a more extensive source inventory. Till now nearly all of the factor analyses have been used to identify sources of various species found in airborne particulate matter such as soil factor, gulf factor, anthropogenic factor, etc. In the present study, using the data of single-particle analysis, 255 individual particles collected during Asian dust storm event were classified by statistical analysis. The purpose of this study is to determine the property of individual Asian dust storm particles and to classify them by multivariate statistical technique and comparison of interelement.

2. Experimental

2.1. Sampling

Particle samplings were performed at Kosan super site in Korea during ACE-Asia. The Kosan site (33.17°N; 126.10°E) is located at the western tip of Cheju Island, Korea. Cheju Island, located on the southwest seas off the Korean peninsula, is the largest island in Korea, covering 1845 km² in area (latitude of 73 km longitude of 41 km). The climate of Cheju Island has features of both subtropical oceanic climate and temperate climates, warm and mild, yet showing distinct seasonal changes. With an average temperature of 16°C (hottest summer: 33.5°C, coldest January: 1°C), Cheju Island has the mildest weather. This sampling site was well described in elsewhere (Kim et al., 1998). The ground-based sampling site at Kosan is about 70 m above sea level and 100 m southwest from the Cheju upper air meteorological

station. Atmospheric aerosols were collected by a 2-stage filter pack sampler in several dust storm events from the end of March 2001 to the end of April 2001. The sampling duration time was 20 min. This sampler collected the coarse and fine fractions of the aerosols separately on a prefilter (a 47 mm diameter, 8 μm rated pore size Nuclepore filter with $1 \times 10^5 \text{ cm}^{-2}$ pore density and 1 mg cm^{-2} nominal wt.) and a back-up filter (a 47 mm diameter, 0.4 μm rated pore size Nuclepore filter with $1 \times 10^8 \text{ cm}^{-2}$ pore density and 1 mg cm^{-2} nominal wt.), respectively. The 50% cut-off diameter of the prefilter with 251 min^{-1} flow rate was estimated to be 1.2 μm equivalent aerodynamic diameter (Kasahara et al., 1996; Ma et al., 2001). The mechanisms by which particles are arrested on the Nuclepore filter are Brownian diffusion, interception, and inertial impaction. Efficiencies for the separation processes relate to the governing variables such as particle size, aerosol approach velocity, and filter pore size (Smith et al., 1976). During the sampling period the range of wind speed was 3.6–20.5 m s⁻¹, and it was generally blowing from the west. The temperature was around 10.1–17.2°C and the average relative humidity in the sampling period was 56%.

2.2. Chemical analysis of individual particles

X-ray microprobe system equipped at Super Photon ring 8 GeV (SPring-8), BL-39XU (at present BL-37XU) was applied to the quantification analysis of the ultra trace elements in the individual coarse particles (>1.2 μm). Hayakawa (2000) had developed this BL-39XU at SPring-8 that chemically analyzes the trace elements from various species. By using this SPring-8, BL-39XU, we can successfully reconstruct elemental maps and analyze multiple elements with fg (femtogram) level sensitivity (Hayakawa et al., 2001). Fig. 1 shows the

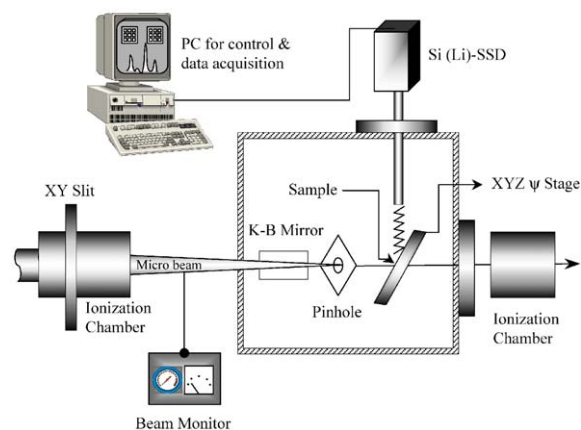


Fig. 1. Schematic illustration of the experimental setup for XRF microprobe at SPring-8, BL-39XU.

schematic illustration of the experimental setup for X-ray fluorescence (XRF) microprobe. To make the X-ray beam narrow with micro scale, a pair of elliptical mirrors (Kirkpatrick and Baez mirror, KB mirror) was installed in the optical path. A combination of the focusing mirror and a fixed exit monochromator enabled energy-tunable X-ray microbeam. The preliminary experimental results show a focal spot down to $2\mu\text{m}(V) \times 4\mu\text{m}(H)$ with the photon flux more than 1×10^{10} photons s^{-1} for monochromatic 10 keV X-ray (Hayakawa et al., 2001). A sample was placed on the XY scanning stage in a vacuum chamber, and the randomly selected sample areas ($500\text{--}1000\mu\text{m}^2$ per one time) were scanned by the microbeam. The takeoff angle of 10° was used for the measurement. The intensity of the incident X-rays was monitored by an ionization chamber. After finishing the scanning processes, the XRF elemental image of aerosol particles can be obtained. And then, the point analysis was carried out according to the coordinates decided from the XRF elemental maps. However, this analysis was restricted to particles whose size was greater than $1\mu\text{m}$. The sizes of the large particles were evaluated from a cross-section of the representative elemental image (e.g. Fe), and the sizes of the particles less than the beam size were estimated from the representative elemental signal on the assumption that the portion of the representative composition was the same among the particles. The fluorescence X-rays were recorded with a Si(Li) detector placed in the electron orbit plane of the storage ring and mounted at 90° to the incident X-rays to minimize background caused by the scattering. To avoid excessive counting rate, the sample–detector distance of 100 mm was used. The more detailed analytical procedures and experimental setup used for XRF microprobe analysis have been described elsewhere (Hayakawa et al., 2001). By means of this XRF analytical technique, 255 particles collected on 8 April 2001 were analyzed.

3. Results and discussion

3.1. Backward trajectory analysis

The transport situation of air parcel during Asian dust storm events was analyzed through backward trajectory starting at Kosan, Cheju based on NOAA (<http://.arl.noaa.gov>) analyzed data at 00 UTC. Three-day backward trajectories originated at a point situated along the 33.17°N ; 126.10°E , were computed at three different altitude levels. Fig. 2 shows the result of backward trajectory for the Asian dust storm event on 8 April 2001 at 3000, 4000, and 5000 m altitude levels. The result of backward trajectory analysis showed that the air parcels were transported to our sampling site through the desert and loess areas in China and

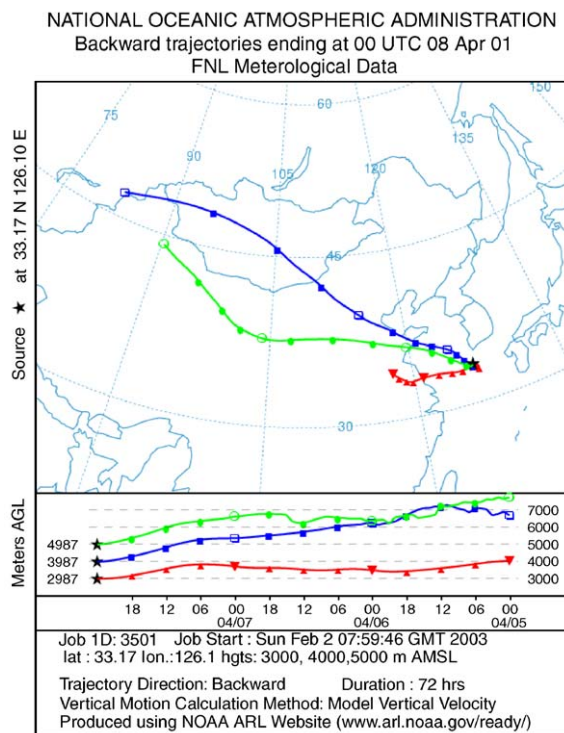


Fig. 2. Backward trajectories for air parcels that arrived at our Kosan super site calculated from NOAA (<http://www.noaa.gov>).

Mongolia plateau. The trajectory map drawn by Hybrid Single-Particle Lagrangian Integrated Trajectory (HYSPPLIT) model, NOAA shows an aerial view of the paths an air parcel took, and a vertical view of its floating at each different altitude. Meters AGL means the height of the air parcel. The height of the air parcel is measured in meters above model ground level (AGL).

3.2. Elemental mass of individual particles

The statistical elemental mass data for 255 individual particles are listed in Table 1. The estimated Cl mass is seen ranging from 4.22×10^{-4} to 6.03×10^{-1} pg with average 1.02×10^{-1} pg and shows the highest average mass. High frequencies of Cl were reported in the area of Japan because Asian dust storm particles were absorbed or coalesced with particles containing sea salt during the long-range transport (Wang and Guanghua, 1996). Dust-originated components like Si, Ca, and Fe followed. They are in the range of 2.01×10^{-3} to 4.58×10^{-1} (average 3.78×10^{-2} pg), 2.73×10^{-4} to 6.83×10^{-1} (average 3.68×10^{-2} pg), and 6.73×10^{-5} to 1.76 pg (average 3.37×10^{-2} pg), respectively. Also sulfur shows significant mass ($\sim 6.50 \times 10^{-1}$ pg) with average 3.11×10^{-2} pg. The mass ratio of [soil components + Cl] to [total elements] is 0.84. This implies that

Table 1
Statistical summary of the masses for 255 particles collected in Asian dust storm event

	Min. (pg)	Max. (pg)	Average (pg)	S.D. (pg)	Median (pg)
Aluminum	1.36E-03	3.45E-01	2.35E-02	3.64E-02	1.23E-02
Silicon	2.01E-03	4.58E-01	3.78E-02	5.45E-02	1.83E-02
Phosphorus	1.50E-11	2.52E-01	1.83E-02	2.88E-02	9.00E-03
Sulfur	4.58E-10	6.50E-01	3.11E-02	6.05E-02	1.35E-02
Chlorine	4.22E-04	6.03E+00	1.02E-01	4.61E-01	2.08E-02
Potassium	3.75E-11	1.94E-01	1.87E-02	2.84E-02	8.57E-03
Calcium	2.73E-04	6.83E-01	3.68E-02	7.04E-02	1.62E-02
Scandium	2.30E-10	7.18E-02	3.78E-03	7.73E-03	1.54E-03
Titanium	5.00E-05	3.40E-01	6.96E-03	2.91E-02	1.11E-03
Vanadium	3.70E-06	1.24E-01	1.73E-03	8.63E-03	3.42E-04
Chromium	1.95E-04	3.87E-02	1.04E-03	2.60E-03	6.45E-04
Manganese	3.04E-05	4.51E-02	1.25E-03	4.26E-03	3.72E-04
Iron	6.73E-05	1.76E+00	3.37E-02	1.32E-01	8.29E-03
Cobalt	1.55E-05	1.21E-01	2.37E-03	9.14E-03	6.06E-04
Nickel	4.30E-06	3.17E-03	1.23E-04	3.06E-04	6.93E-05
Copper	2.22E-03	1.96E-02	2.92E-03	1.25E-03	2.76E-03
Zinc	3.78E-06	1.80E-01	1.53E-03	1.14E-02	2.27E-04

the effect of soil and sea-salt components on total elements mass is significant. While on the other hand, the several anthropogenic elements like V, Cr, Mn, Co, Ni, Cu, and Zn show poor elemental masses as shown in Table 1.

3.3. Factor analysis for particle classification

As mentioned earlier, though as one of the multivariate statistical techniques such as cluster analysis and principal component analysis, factor analysis is commonly used in environmental studies to deduce sources from data taken at receptors; the main application of factor analysis is to reduce the number of variables. Therefore, factor analysis can be applied as a data reduction method. In this study, factor analysis was applied to the grouping of individual particles (i.e. variables) according to their elemental components. Factor analysis was performed by 255 variables (the number of individual particles) and 17 cases (elemental components) namely, 255×17 matrix of correlation coefficients was constructed. In this study, the procedure of factor analysis is as follows: choosing the variables and cases (the number of variables and cases)—Choosing the factoring method (extraction method and the number of factors)—Construction of the matrix of correlation coefficients—Factor rotating (Varimax with Kaiser normalization)—Estimation of the rotating result—Calculation of factor score. Components in our data set had the missing value of 0.5–2%. Missing data pose problems for factor analysis because the program requires complete matrices. Missing data can be replaced in various ways. Genuinely missing data, whose values cannot be estimated reliably, are commonly

replaced with mean values of their elements. Detection limits can be replaced by some constant fraction of their values (usually one-half) or by some random fraction. In this study, missing data were substituted by mean values. The factor loadings are shown in Table 2. Most of the individual particles (222 particles) were successfully grouped into four factors. The percents of variance for each factor are 29.9, 27.5, 19.1, and 10.9 for factors 1, 2, 3, and 4, respectively, with 87.4% of the cumulative (factor 1–4). Thirteen particles, roughly 5% of the total 255 particles, were not classified by four factors. These particles were measured poorly and have little source-identification power. Eighty-six individual particles (from particle number 140 to 47 in Table 2) show high factor loading on factor 1. These particles consist of overwhelmingly high Cl mass with very slight S. In factor 2, eighty-one individual particles containing absolutely high masses for crustal components (Si, P, K, and Al) were classified. The third factor seems to express the modification of Asian dust storm particles, since it is correlated with Ca, Cl, and S. This modification by multiple elements was found in and/or on forty-nine particles. The fourth factor grouped by 25 particles depends upon Fe, Cl, and Al. They are the predominant elemental components of soil and marine originated particles.

Table 3 summarizes the factor loadings with probable source types. Also though the spectra of several minor components are not clearly distinguished as one of the example particles classified in each factor, the XRF spectra of 4-particle ($> 1.2 \mu\text{m}$) are drawn in Fig. 3. Four source categories, which explain most of the individual particles (95% of total particles), were identified. Roughly 61% of the particles collected during

Table 2
Varimax-rotated factor loadings for the elemental masses of 255 particles collected in Asian dust storm event

Particle no.	Factor 1	Factor 2	Factor 3	Factor 4
P140	0.994	0.001	0.084	0.055
P107	0.994	0.027	0.081	0.055
P16	0.994	-0.049	0.049	0.046
P12	0.993	-0.045	0.087	0.039
P15	0.992	-0.052	0.073	0.043
P254	0.992	-0.038	0.096	0.046
P136	0.992	-0.022	0.026	0.067
P159	0.989	0.069	0.109	0.050
P104	0.981	0.032	0.147	0.055
P132	0.980	0.012	0.190	0.042
P131	0.979	0.087	0.151	0.040
P247	0.972	0.013	0.060	0.208
P129	0.972	0.031	0.223	0.040
P105	0.967	0.159	0.177	0.070
P90	0.963	0.022	0.065	0.094
P70	0.963	0.185	0.077	0.137
P17	0.956	0.043	0.266	0.110
P158	0.955	0.068	0.262	0.072
P14	0.948	0.174	0.170	0.053
P109	0.946	0.108	0.152	0.021
P61	0.943	0.091	0.209	0.044
P46	0.937	0.195	0.110	0.252
P182	0.931	0.153	0.321	0.020
P27	0.930	0.264	0.151	0.158
P180	0.928	0.137	0.167	-0.003
P240	0.925	0.131	0.198	0.050
P183	0.920	0.018	0.261	0.017
P142	0.910	0.260	0.248	0.175
P93	0.908	0.104	0.236	0.015
P6	0.906	0.323	0.145	0.084
P238	0.892	0.324	0.227	0.078
P108	0.885	0.164	0.377	0.130
P121	0.880	-0.028	0.351	0.000
P220	0.875	0.252	0.330	0.197
P249	0.870	0.127	0.063	0.419
P237	0.869	0.362	0.235	0.080
P11	0.867	0.409	0.092	0.004
P10	0.866	0.294	0.270	0.031
P248	0.865	0.016	0.474	0.101
P143	0.865	-0.005	0.465	0.023
P39	0.864	0.136	0.176	0.054
P106	0.859	0.019	0.270	-0.001
P127	0.857	0.333	0.350	0.088
P88	0.857	-0.009	0.018	0.106
P245	0.856	0.125	0.332	0.031
P190	0.846	0.364	0.244	0.280
P205	0.828	0.002	0.525	0.012
P111	0.820	0.165	0.473	0.092
P235	0.806	0.375	0.183	0.115
P202	0.801	0.354	0.310	0.165
P57	0.795	0.143	0.236	0.042
P13	0.792	0.322	0.309	0.065
P96	0.790	0.093	0.590	0.016
P133	0.782	0.367	0.031	0.187
P171	0.776	0.018	0.617	0.062
P163	0.772	0.432	0.391	0.157
P252	0.757	0.157	0.504	0.085
P20	0.755	0.460	0.288	0.306
P244	0.754	0.500	0.345	0.012
P76	0.746	0.178	0.617	0.060
P56	0.733	0.205	0.643	0.042
P74	0.728	0.492	0.251	0.200

Table 2 (continued)

Particle no.	Factor 1	Factor 2	Factor 3	Factor 4
P52	0.724	0.337	0.587	0.116
P89	0.723	0.468	0.312	0.077
P231	0.709	0.311	0.393	0.106
P181	0.705	0.615	0.162	0.051
P255	0.703	-0.029	0.367	0.347
P139	0.702	0.610	0.246	0.048
P232	0.701	0.450	0.245	0.190
P95	0.689	0.479	0.164	0.214
P24	0.687	0.280	0.543	0.060
P157	0.675	0.482	0.141	0.522
P219	0.667	0.380	0.541	0.263
P188	0.662	0.277	0.523	0.430
P239	0.660	0.142	0.588	0.027
P221	0.660	0.389	0.566	0.272
P225	0.645	0.546	0.191	0.261
P241	0.619	0.296	0.610	0.043
P120	0.607	0.492	0.472	0.090
P60	0.593	0.193	0.536	0.256
P230	0.593	0.384	0.475	0.081
P54	0.576	0.415	0.395	0.495
P63	0.568	0.565	0.406	0.182
P253	0.553	-0.034	0.439	0.522
P128	0.549	0.373	0.547	0.102
P47	0.535	0.442	0.476	0.383
P161	0.185	0.974	0.041	-0.042
P153	0.013	0.973	-0.002	0.090
P80	0.042	0.972	0.079	0.032
P147	0.172	0.968	0.074	0.122
P193	0.158	0.966	0.121	0.047
P141	0.121	0.964	0.146	0.059
P69	0.180	0.944	0.100	0.138
P122	0.093	0.942	0.064	0.040
P68	0.158	0.935	0.217	0.151
P29	0.203	0.926	0.238	0.106
P148	0.252	0.925	0.144	0.064
P222	0.269	0.918	0.175	0.117
P189	0.284	0.917	0.056	0.194
P31	-0.027	0.910	0.017	0.117
P155	0.088	0.901	0.275	0.302
P9	0.026	0.899	0.361	0.052
P194	0.039	0.896	0.034	-0.009
P229	0.153	0.889	0.340	0.253
P4	0.016	0.879	0.386	0.229
P211	0.065	0.863	0.147	0.465
P8	0.056	0.855	0.429	0.269
P208	0.229	0.853	0.142	0.371
P115	0.243	0.848	0.417	0.202
P100	0.005	0.843	0.069	0.155
P35	0.311	0.842	0.184	0.247
P22	0.102	0.841	0.460	0.250
P209	0.227	0.833	0.166	0.001
P72	0.105	0.827	0.448	0.276
P212	0.068	0.826	0.259	0.479
P26	0.039	0.821	-0.015	-0.024
P85	0.494	0.817	0.120	0.046
P156	0.136	0.810	0.097	0.170
P145	0.244	0.807	0.345	0.096
P58	0.199	0.798	0.179	0.498
P162	0.190	0.792	0.220	0.394
P154	0.020	0.791	0.137	0.426
P204	0.191	0.790	0.328	0.087
P112	0.319	0.785	0.376	0.249
P18	-0.059	0.781	0.017	0.276
P250	0.426	0.780	0.191	0.374

Table 2 (continued)

Particle no.	Factor 1	Factor 2	Factor 3	Factor 4
P150	0.009	0.777	0.144	0.430
P110	0.031	0.777	0.096	0.519
P48	0.079	0.776	0.204	-0.159
P34	0.284	0.776	0.164	0.249
P62	0.168	0.772	0.476	0.361
P33	-0.060	0.765	0.062	0.071
P151	0.013	0.765	0.150	0.446
P149	0.014	0.762	0.120	0.495
P123	0.203	0.759	0.261	0.212
P103	0.324	0.749	0.265	0.190
P5	0.053	0.746	0.048	-0.076
P168	0.138	0.745	0.207	0.538
P38	0.100	0.740	0.649	0.098
P75	0.176	0.737	0.611	0.093
P206	0.292	0.730	0.250	0.133
P64	0.192	0.692	0.489	0.450
P2	0.169	0.689	0.504	0.304
P144	0.185	0.685	0.545	0.107
P30	0.054	0.684	0.217	0.369
P169	0.357	0.683	0.383	0.414
P81	0.113	0.683	0.492	0.502
P32	0.256	0.680	0.436	0.397
P197	0.089	0.677	0.388	0.591
P91	0.119	0.676	0.130	0.504
P113	0.667	0.670	0.252	0.167
P114	0.594	0.669	0.235	0.090
P152	0.185	0.669	0.623	0.344
P7	0.582	0.667	0.239	0.045
P124	0.633	0.661	0.239	0.161
P195	0.354	0.658	0.279	0.599
P134	0.218	0.653	0.509	0.142
P242	0.465	0.650	0.341	0.412
P1	0.356	0.647	0.345	0.005
P201	0.419	0.642	0.525	0.151
P167	0.215	0.633	0.485	0.482
P191	0.538	0.628	0.135	0.265
P138	0.184	0.625	0.577	0.249
P42	0.383	0.624	0.483	0.140
P23	-0.099	0.624	-0.061	0.487
P37	0.312	0.610	0.481	0.150
P234	0.471	0.539	0.490	-0.031
P166	0.253	0.067	0.956	0.103
P175	0.285	-0.037	0.951	-0.005
P210	0.296	0.044	0.936	0.167
P174	0.384	0.028	0.917	0.050
P172	0.388	0.021	0.915	0.049
P213	0.251	0.330	0.898	0.104
P236	0.409	0.169	0.889	0.107
P224	0.295	0.250	0.889	0.106
P84	0.179	0.315	0.888	0.233
P186	0.203	0.299	0.884	0.109
P97	0.249	0.128	0.869	0.094
P185	0.364	0.285	0.865	0.021
P125	0.310	0.389	0.853	0.027
P83	0.407	0.187	0.830	0.288
P223	0.199	0.418	0.821	0.063
P102	0.531	0.115	0.802	0.108
P118	0.170	0.178	0.783	0.068
P217	0.194	0.137	0.766	0.588
P165	0.431	0.267	0.766	0.346
P170	0.389	0.339	0.764	0.149
P233	0.347	0.496	0.763	0.197
P25	0.083	0.633	0.762	0.026
P198	0.407	0.192	0.762	0.021

Table 2 (continued)

Particle no.	Factor 1	Factor 2	Factor 3	Factor 4
P218	0.286	0.543	0.745	0.200
P200	0.358	0.186	0.742	0.012
P177	0.083	0.601	0.728	0.205
P207	0.660	0.005	0.727	0.009
P86	0.260	0.569	0.725	0.150
P126	0.363	0.456	0.712	0.384
P3	0.660	0.219	0.694	0.014
P71	0.654	0.077	0.687	0.050
P98	0.212	0.348	0.683	0.189
P160	0.362	0.463	0.674	0.383
P28	0.207	0.592	0.668	0.249
P66	0.441	0.566	0.668	0.170
P45	0.514	0.232	0.635	0.001
P77	0.212	0.426	0.633	0.104
P199	0.604	0.321	0.632	0.326
P203	0.424	0.472	0.627	0.152
P44	0.346	0.426	0.622	0.161
P94	0.608	0.301	0.617	-0.023
P50	0.363	0.248	0.616	0.307
P119	0.398	0.404	0.616	0.074
P135	0.096	0.434	0.613	0.606
P82	0.345	0.504	0.599	0.184
P41	0.249	0.524	0.596	0.479
P137	0.081	0.492	0.577	0.531
P227	0.526	0.512	0.572	0.178
P101	0.306	0.544	0.546	-0.010
P246	0.016	0.014	0.035	0.995
P243	0.172	0.009	0.028	0.984
P215	0.161	0.053	-0.022	0.980
P73	-0.025	0.181	-0.006	0.975
P228	0.329	0.031	0.157	0.916
P67	-0.034	0.426	0.200	0.875
P65	-0.022	0.423	0.215	0.872
P49	-0.068	0.431	-0.004	0.869
P79	0.206	0.458	0.188	0.838
P78	0.345	0.306	0.189	0.837
P21	-0.020	0.497	-0.089	0.826
P216	-0.059	0.519	0.275	0.802
P178	0.201	0.488	0.239	0.792
P192	0.194	0.269	0.443	0.743
P214	0.684	0.077	0.076	0.717
P43	0.052	0.606	0.073	0.708
P196	0.634	0.267	0.133	0.707
P187	0.193	0.643	0.192	0.704
P99	0.066	0.592	0.392	0.679
P251	0.501	0.345	0.227	0.650
P19	-0.034	0.609	0.139	0.629
P40	0.422	0.422	0.339	0.601
P176	0.216	0.528	0.532	0.580
P87	0.529	0.285	0.199	0.576
P92	0.560	0.377	0.468	0.564
% of Variance	29.9	27.5	19.1	10.9
Cumulative %	29.9	57.4	76.5	87.4

Extraction method: Principal component analysis. Rotation method: Varimax with Kaiser normalization. Non-classified particles by four factors: P117, P36, P55, P53, P226, P173, P59, P130, P146, P164, P184, P116, P179, P51.

Table 3
Factors derived from the data set of 255-variable \times 17-element and probable source types

	Characteristic element in factor	Number of particles	% of the total particle number	Probable source type
Factor 1	Cl (mixed with very low S)	86	33.73	Marine
Factor 2	Si, P, K, Al	81	31.76	Crustal
Factor 3	Ca, Cl, S	49	19.22	Crustal + Marine + Sulfur
Factor 4	Fe, Cl, Al	25	9.80	Crustal + Marine

Asian dust storm event at Kosan contain crustal component with relatively pure (particle #153 in Fig. 3), mixed with marine/S (particle #175 in Fig. 3), and mixed with marine (particle #215, #243 in Fig. 3). It is considered that approximately 32% of the Asian dust storm particles collected at Kosan are not greatly modified. On the other hand, particles including marine components (pure, mixed with crustal/S, and mixed with crustal) account for 63% of the total particle population. On the basis of these results, although detailed information like the air parcel movement in the inland of China and the elemental individual composition of desert soil is needed, we can assume that roughly 19% of the Asian dust storm particles contain S. For the S contained in Asian dust storm particle, it is necessary to discuss in detail. As suggested by Hseung and Jackson (1952), the desert soil collected at the desert area in China has a relative fraction of S in the form of CaSO_4 . Ma et al. (2001) reported that the significant concentration of S in coarse fraction particles collected in Kyoto, Japan during Asian dust storm event was detected in both single particles and bulk samples. For the S contained in coarse mode particles, it is suggested that it originated from both CaSO_4 in the desert soil and the anthropogenic S in the form of H_2SO_4 . For the purpose of discussing this S, the simple interelemental mass ratio of S to Ca can be applied. As mentioned previously, S coexisted with Ca and Cl in the 49 particles (19% of the total particle population) grouped in factor 3. About 21% of the particles in factor 3 have S/Ca ratio, 11.14. However, the mean S/Ca mass ratio for 79% of the particles was found to be relatively low, 0.44. On the basis of this S/Ca ratio, it can be said that a small part of the CaCO_3 in Asian dust storm particles would be converted to CaSO_4 through the chemical reaction between CaCO_3 and H_2SO_4 during long-range transport. Moreover, we can assume that this modification of Asian dust storm particles would occur in the urban and industrial areas of China. Another possible process is the gas-to-particle conversion of SO_x on the dust particle surface during transport in the air. The westerly prevailing wind and the longitudinal mixing between air masses in accordance with the arrangement of high- and low-pressure systems contribute to the mixing processes among dust particles, sea salt, and anthro-

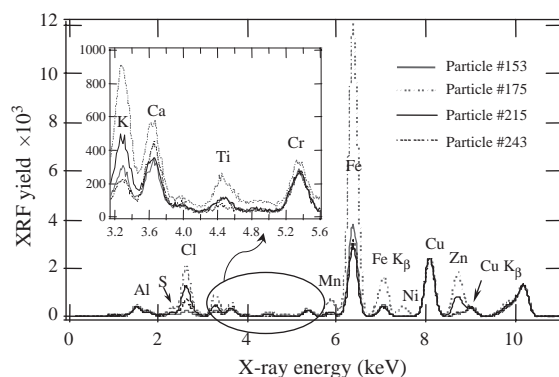


Fig. 3. XRF spectra of the individual 4-particle ($>1.2\mu\text{m}$) collected in Asian dust storm event on 8 April 2001.

pogenic aerosol precursors (Song and Carmichael, 1999). Added to this, at least a part of these CaSO_4 particles are of marine origin because CaSO_4 would be produced by fractional crystallization of marine aerosol (Andreae et al., 1986). Furthermore, the interaction of airborne CaCO_3 either from marine or biogenic origin with SO_2 or H_2SO_4 could explain the formation of CaSO_4 .

3.4. Mixing state of Asian dust storm particles with sea salt

To estimate the mixing state of Asian dust storm particles with sea salt, Si, Cl, Ca, and Fe were mapped from a scan area of $250\mu\text{m} \times 250\mu\text{m}$. Furthermore, we plotted four kinds of elemental masks that correspond to each particle found within a scan area in Fig. 4. From these four elemental maps and their masks replayed corresponding to individual particles, particles were categorized into two groups, namely internally mixed particles and externally mixed particles. As the typical internally mixed particle, the particle numbers of 967, 34, 50, and 60 in the elemental maps of Si, Cl, Ca, and Fe, respectively, are present at the same place around row 85-column 190 pixel number in Fig. 4. Also many other particles containing Cl are mixed with singular and plural mineral components (row 145-column 47, row 112-column 125, row 132-column 170, and row

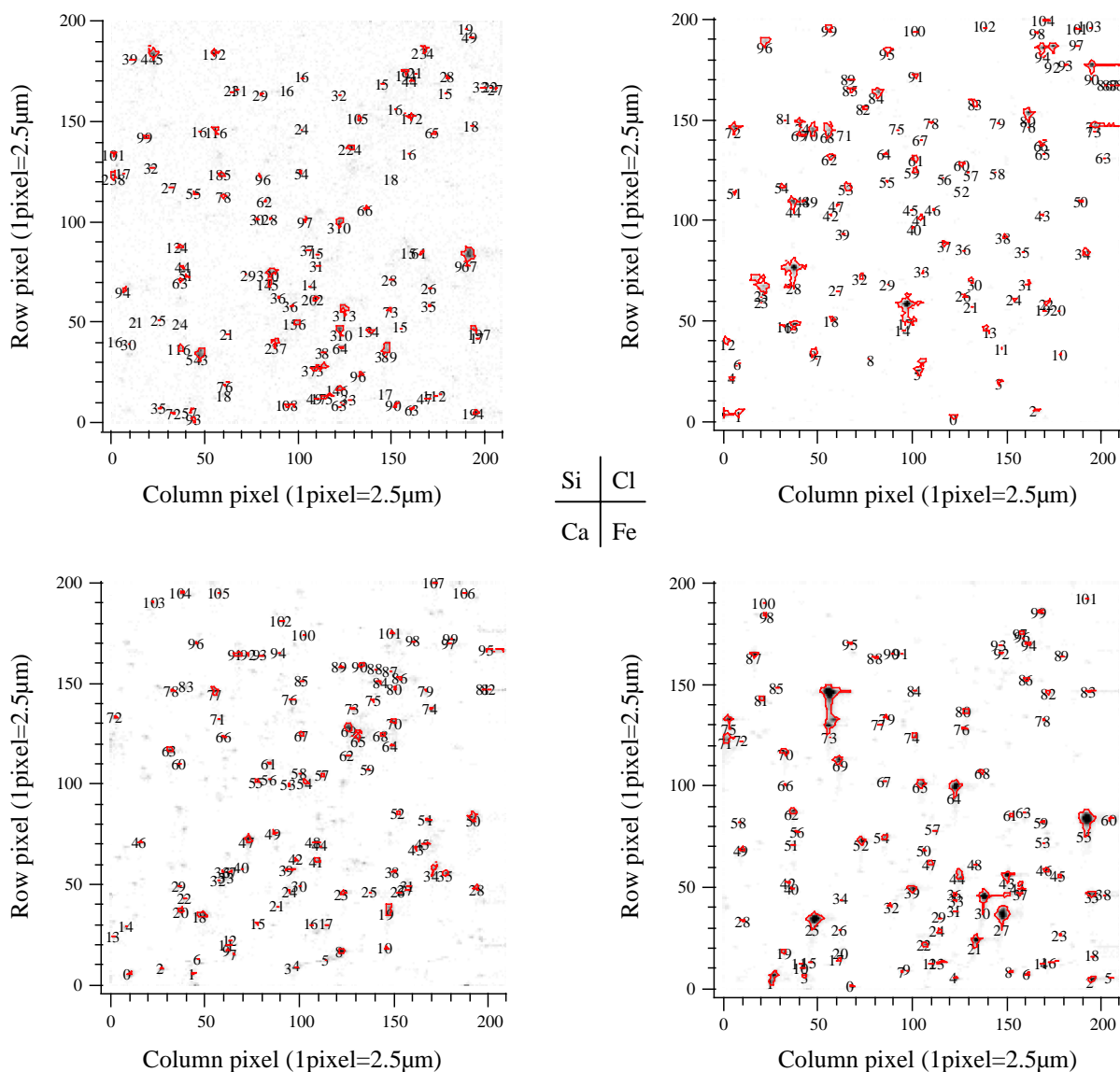


Fig. 4. Si, Cl, Ca, and Fe XRF images of the individual particles collected in Asian dust storm event. 10 keV X-ray was applied for excitation.

55-column 177). On the contrary, in Fig. 5, a masking comparison shows that the particles containing Cl are present separated from those containing soil components. For example, some particles indicated by a triangle mark in the mask (row 110-column 190, row 102-column 167, row 92-column 62, and row 195-column 137) are present alone without overlapping.

Though there remains the need to more fully understand how Asian dust storm particles age and how anthropogenic pollutants are incorporated into these dust and marine particles, as the several mechanisms for the internal mixture of Asian dust storm particles with

sea salt, Brownian coagulation, impaction by differential sedimentation, and coalescence of cloud droplets containing minerals with those containing sea salt can be considered. But Andreae et al. (1986) and Friedlander and Smoke (1977) reported that Brownian coagulation and impaction by differential sedimentation cannot explain internal mixture in particles with diameter of 2–4 μm during long-range transport. Therefore, the internal mixture of Asian dust storm particles with sea salt in our sampling period probably occurred by the cloud condensation nuclei in an atmosphere with low supersaturation. Cloud droplets should form

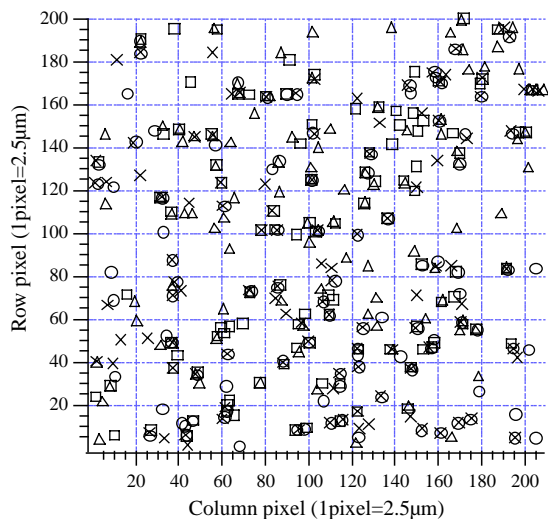


Fig. 5. Mixing state of Fe, Ca, Si, and Cl in individual particles. Circle, trapezium, cross, and triangle mean Fe, Ca, Si, and Cl, respectively.

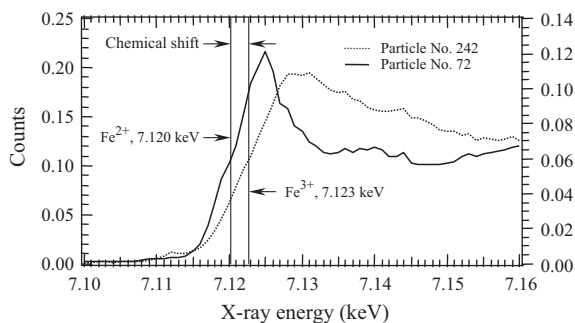


Fig. 6. Normalized Fe K-edge XANES spectra of two Fe-rich particles (particle #247 and 72) collected in Asian dust storm event.

individually on the Asian dust storm particles and sea-salt particles in the marine boundary layer. Then the internal mixing of dust particles with marine particles should occur on the evaporation of the cloud droplets.

3.5. Determination of the chemical state of Fe based on XANES technique

The fine structure in the immediate vicinity of the X-ray absorption edge is sensitive to the valence of the absorber atom and the site geometry. This near-edge feature is referred to as an X-ray absorption near edge structure (XANES) (Nakai et al., 1998). The energy of the absorption edge is the minimum energy required to excite an electron from a deep core state to an empty

bound state or to a continuum state. The chemical state of an element affects the XANES structure, especially the relative position of the absorption edge, which is known as the chemical shift (Nakai et al., 1998). The mapping of chemical state based on this XANES technique can produce the isolated maps of Fe^{2+} and Fe^{3+} ions in a sample. Fig. 6 shows the normalized Fe K-edge XANES spectra of two Fe-rich particles (particle #247, #72). The XANES spectrum was calculated by normalizing the intensity of the fluorescent X-rays with that of the incident X-rays and by plotting against the X-ray energy. As shown in Fig. 6, the chemical forms of Fe (Fe^{2+} , Fe^{3+}) can be clearly characterized by its K-edge micro-XANES spectra. It is found that the absorption edge shifts to a higher energy as the valence state of Fe in particles increases. In Fig. 6, the chemical shift between Fe^{2+} and Fe^{3+} was about 3 eV. Fe^{2+} and Fe^{3+} were mainly excited by X-rays with the energies of 7.120 and 7.123 keV, respectively. A total of 13 XANES spectra were drawn for 13 Fe-rich particles. Fe^{3+} can be considered the main chemical state of Fe in particles collected in Asian dust storm accounting for 73% of the particles.

3.6. Source identification for trace heavy metals

Though it was negligible mass level relative to those of other major elements, the particles containing heavy metals were often found. Also several heavy metals were relatively regularly detected. Source identification for these minor trace heavy metals was made using the enrichment factor (EF) and the interelemental correlation coefficient shown in Fig. 7. The comparison between the elemental concentration levels of atmospheric aerosols when they are higher than expected in their natural form, according to their proportion in the natural origins, is a simple way to identify their source origin (Gregory et al., 1978; Scheff and Valiozis, 1990). The degree of enrichment of trace elements in particles is given by an EF. To quantify enrichment, Rahn (1976) proposed the use of enrichment factors, which is defined as: $\text{EF}_x = ((C_{x,p}/C_{\text{ref},p})/(C_{x,c}/C_{\text{ref},c}))$, where, $C_{x,p}$ and $C_{\text{ref},p}$ are the concentrations of the element and of a suitably chosen reference element in the atmospheric particle, respectively, and $C_{x,c}$ and $C_{\text{ref},c}$ are the concentrations of the element and of a reference element in the soil. The soil components are based on the data reported by Scheff and Valiozis (1990). As a result, every minor trace heavy metal had very high EFs. EF values for V, Cr, Ni, Cu, and Zn are 74.5, 69.7, 19.6, 26.0, and 299.8, respectively. Moreover, the plotting of these elements vs. soil-originated elements shows no good correlation coefficients. Owing to the maximum levels for several trace heavy elements like Ti, V, Cr, and V, their mass levels are shown to be nearly as constant for all particles in the scattering plot matrix of Fig. 7. Zn is

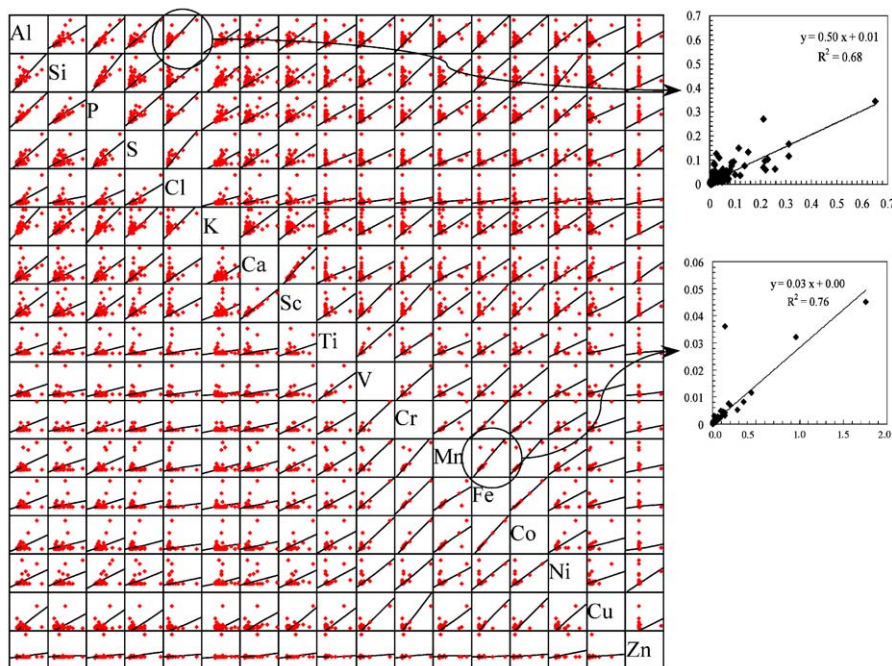


Fig. 7. Correlation coefficient matrix among 17-element analyzed from 255-particles.

mainly emitted from iron, steel or ferro-alloys plants (Pacyna, 1984), as the other sources for Zn are refuse incineration (Mamame, 1988) and tire wear (Hopke, 1985). Cr is regarded as an indicator of emission from the steel and iron industry (Pacyna, 1984). V- and Ni-bearing particles are dominated by the burning of residual fuel oil and other oil-fired units (Mroz, 1976; Zoller et al., 1973). Gregory et al. (1978) noted that the major sources of Cu on particles in the urban site are coal/oil/refuse. Also they classified soil as a minor source of Mn. Even though EF value of Mn was found to be more or less low (9.1), the correlation coefficient between Mn and crustal components was very low. However, the plotting of Mn vs. Fe shows a good correlation with $R^2=0.76$. Thus we cannot exclude the possibility that Mn was derived from iron industry. As a previous study (Kim et al., 1998) already pointed out, Kosan is one of the remote sites. From this point of view, even though there is no evident local sources information at the inland of China for these trace heavy metals, it is suggested that they were affected by the air masses passed directly over the industrial areas of China.

4. Summary

The primary goal of this study is to determine the properties of individual Asian dust storm particles. An intensive field measurement was performed at the Kosan

super site of ACE-Asia located on the west coast of Cheju Island, Korea. The chemical analysis of ultra trace elements in the individual coarse particles ($>1.2\mu\text{m}$) was carried out by the X-ray microprobe system installed at SPring-8. The following results are a summary of this study.

Approximately 34% of the total particle population was found to be high factor loading on factor 1 showing sea-salt rich component. In factor 2, roughly 32% of the particles containing absolutely high mass for crustal components were classified. Factor 3 (19% of the total particle population) and factor 4 (10% of the total particle population) seem to express the modification of Asian dust storm particles. By means of XRF elemental maps and elemental masks replayed corresponding to individual particles, particles were categorized into two groups, namely internally and externally mixed particles. Fe^{3+} can be considered the main chemical state of Fe in Asian dust storm particles collected during our sampling period. Several minor heavy metals showing negligible elemental masses in comparison with those of other major elements were probably affected by the air masses passed directly over the industrial areas of China.

Although, in the present study, the quantification of elemental mass for 17-element (major and trace) was successfully performed; however, several attempts have to be subsequently made as for further study. For example, the calculation of single particle volume using scattering characteristics, the separated elemental ana-

lysis between surface and inner portions of a single particle can be suggested. Also as one of the visualization methods for the three-dimensional chemical inner structure of a single particle, the XRF tomography technique introduced by Ma et al. (2002) can be applied in the future.

Acknowledgements

This study was supported in part by funds from the Grant-in-Aid for Scientific Research on Priority Areas under Grant Nos. 14048212 and 14048213 from Ministry of Education, Culture, Sports, Science and Technology (MEXT), Japan. The synchrotron radiation experiments were performed at the SPring-8 with the approval of the Japan Synchrotron Radiation Research Institute (JASRI) (Proposal No. 2002B0395-NOS-np, 2002A4029-LM-np). The authors also express sincere thanks to Mr. C.-S. Hong, Air Quality Laboratory of K-JIST, Korea for his sampling support. Finally we thank the anonymous reviewers for their helpful comments.

References

- Andreae, M.O., Charlson, J.C., Bruynseels, F., Storms, H., Van Grieken, R., Maenhant, W., 1986. Internal mixture of sea salt, silicates and excess sulfate in marine aerosols. *Science* 232, 1620–1623.
- Christof, J.K., Thomas, H.P., David, F., Thomas, W.S., Hemphill, M.W., 1992. Factor analysis of trend in Texas acidic deposition. *Atmospheric Environment* 26A, 1137–1146.
- Friedlander, S., Smoke, L., 1977. *Dust and Haze: Fundamentals of Aerosol Behavior*. Wiley, New York, pp. 317–325.
- Gregory, S.K., Carl, E.C., Glen, E.G., 1978. Chemical element balances and identification of air pollution sources in Washington, DC. *Atmospheric Environment* 12, 1143–1153.
- Hayakawa, S., 2000. X-ray fluorescence method for trace analysis and imaging. *Journal of Japanese Society for Synchrotron Radiation Research* 13, 313–318 (in Japanese).
- Hayakawa, S., Tohno, S., Takagawa, K., Hamamoto, A., Nishida, Y., Suzuki, M., Sato, Y., Hirokawa, T., 2001. Ultra trace characterization using an X-ray microprobe at SPring-8 BL39XU. *Analytical Science* 17, i115–i117.
- Hopke, P., 1985. *Receptor Modeling in Environmental Chemistry*. Wiley, New York, pp. 15–30.
- Hseung, Y., Jackson, M.L., 1952. Mineral composition of the clay fraction of some main soil groups of china. *Soil Science Society of America Journal* 16, 97–110.
- Huang, S., Rahn, K.A., Arimoto, R., 1999. Testing and optimizing two factor-analysis techniques on aerosol at Narragansett, Rhode Island. *Atmospheric Environment* 33, 2169–2185.
- Kasahara, M., Park, J.H., Chatani, S., 1996. Size distribution and solubility of 15 elements in atmospheric aerosols. *International Journal of PIXE* 6, 299–310.
- Kim, Y.P., Lee, J.H., Baik, N.J., Kim, J.Y., Shim, S.G., Kang, C.H., 1998. Summertime characteristics of aerosol composition at Cheju Island, Korea. *Atmospheric Environment* 32, 3905–3915.
- Lowenthal, D.H., Rahn, K.A., 1987. Application of the factor-analysis receptor model to simulated urban- and regional-scale data set. *Atmospheric Environment* 21, 2005–2013.
- Ma, C.J., Kasahara, M., Höller, R., Kamiya, T., 2001. Characteristics of single particles sampled in Japan during the Asian dust storm period. *Atmospheric Environment* 35, 2707–2714.
- Ma, C.J., Tohno, S., Kasahara, M., Hayakawa, S., 2002. A new attempt to visualize the three-dimensional chemical inner-structure of a single raindrop using XRF tomography. The 19th Symposium on Aerosol Science and Technology, Kyoto, Japan, 6–8 August, pp. 129–130 (in Japanese).
- Mamame, Y., 1988. Estimate of municipal incinerator contribution to philadelphia aerosol. I. Source analysis. *Atmospheric Environment* 22, 2411–2418.
- Mroz, E.J., 1976. The study of the elemental composition of particulate emissions from an oil-fired power plant. Ph.D. Thesis, University of Maryland.
- Nakai, I., Numako, C., Hayakawa, S., Tsuchiyama, A., 1998. Chemical speciation of geological samples by micro-XANES techniques. *Journal of Trace and Microprobe Techniques* 16 (1), 87–98.
- Olmez, I., Beal, J.W., Villalume, J.F., 1994. A new approach to understanding multiple-source groundwater contamination: factor analysis and chemical mass balances. *Water Research* 28, 1095–1101.
- Pacyna, J., 1984. Estimation of atmospheric emissions of trace elements from anthropogenic sources in Europe. *Atmospheric Environment* 18, 41–50.
- Rahn, K.A., 1976. The chemical composition of the atmospheric aerosol. Technical Report, University of Rhode Island.
- Scheff, P.A., Valiozis, C., 1990. Characterization and source identification of respirable particulate matter in Athens, Greece. *Atmospheric Environment* 24A, 203–211.
- Smith, T.N., Phillips, C.R., Melo, O.T., 1976. Diffusive collection of aerosol particles on Nuclepore membrane filter. *Environmental Science and Technology* 10, 274–277.
- Song, C.H., Carmichael, G.R., 1999. The aging process of naturally emitted aerosol (sea-salt and mineral aerosol) during long range transport. *Atmospheric Environment* 33, 2203–2218.
- Wang, X., Guanghua, Z., 1996. Some characteristics of the aerosol in Beijing. *International Journal of PIXE* 6, 361–365.
- Zoller, W.H., Gordon, G.E., Gladney, E.S., Jones, A.G., 1973. The sources and distribution of vanadium in the atmosphere. In: *Geochemical Cycles of Trace Elements in Our Environment*, Advances in Chemistry Series, vol. 123, pp. 31–47, American Chemical Society, Washington, USA.